



Nina Feldhofer, BSc

Two-Dimensional Silicon Based Photonic Structures for Improvement of Hybrid Solar Cell Performance

MASTER'S THESIS

To achieve the university degree of
Diplom - Ingenieurin
Master's degree programme: Advanced Materials Science

submitted to

Graz University of Technology

Supervisors

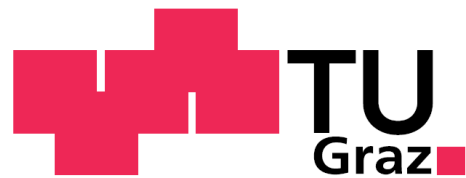
Dipl.-Phys. Dr.rer.nat. Bettina Friedel
Institute of Solid State Physics - TU Graz

Co-Supervisors

Univ.-Prof. Ph.D. Peter Hadley
Institute of Solid State Physics - TU Graz

October 24, 2016

In cooperation with



MAX-PLANCK-INSTITUT
für die Physik des Lichts

EIDESSTATTLICHE ERKLÄRUNG

AFFIDAVIT

Ich erkläre an Eides statt, dass ich die vorliegende Arbeit selbstständig verfasst, andere als die angegebenen Quellen/Hilfsmittel nicht benutzt, und die den benutzten Quellen wörtlich und inhaltlich entnommenen Stellen als solche kenntlich gemacht habe. Das in TUGRAZonline hochgeladene Textdokument ist mit der vorliegenden Masterarbeit/Diplomarbeit/Dissertation identisch.

I declare that I have authored this thesis independently, that I have not used other than the declared sources/resources, and that I have explicitly indicated all material which has been quoted either literally or by content from the sources used. The text document uploaded to TUGRAZonline is identical to the present master's thesis/diploma thesis/doctoral dissertation.

Datum / Date

Unterschrift / Signature

Acknowledgement

First of all I have to thank Sebastian Schmitt so much for his help. Even though he was preparing for his doctoral viva he always had time and patience to support me with great ideas and solutions to my problems.

Special thanks to Sara Jäckle who helped me greatly with her advice and encouragement. Without Silke Christiansen this master thesis would not have been possible. Thank you for your support.

I had the honor and pleasure to work with so many wonderful people from the Max Planck Institute: Manuela Göbelt, Anna Mittelbach, Nino Peer, Pascal Büttner, Michael Latzl and many more. Thank you all for being so supportive, I really enjoyed working with you.

Because of the great input and help from the 'self-assembled materials and structures' group of the FAU especially Marcel Rey and Nicolas Vogel I could successfully finish my work. Thank you very much for all the insight and your patience answering all my questions.

Great thanks to Peter Hadley and Bettina Friedel who had great trust in me and would answer all my mails promptly. Thanks for the great advice and support.

I have to give very special thanks to Astrid Wischgala! She made all the bureaucratic stuff so easy and always had an open ear if any problems occurred.

I could not have done this work without the support and constant encouragement of my friends. I just have to mention all the great people especially Alexandra Müller, Magdalena Truger, Ramona Köppl, Harald Thommesen and Christof Jell.

I would particularly like to thank my whole family for enabling me to study and, more importantly, for their unconditional support and love throughout all my live.

Thank you so much for everything Gerald.

Abstract

Solar energy is a great alternative for conventional energy production. It provides an environmental friendly and sustainable energy source.

While the market is focused nowadays on crystalline solar cells, hybrid solar cells join the great advantages of crystalline and organic solar cells. The major drawback is that hybrid solar cells still show less efficiencies than pure crystalline silicon solar cells.

The purpose of this study was to manufacture and characterize nanostructured hybrid solar cells as these nanostructures in hybrid solar cells might provide higher efficiencies. Solar cells with different nanowires have been produced and the influence of the nanowire size considering the solar cell behavior has been analyzed. The nanostructures have been manufactured by a top down process that has been further optimized in this work. This process can easily be adjusted so that the nanostructures fit every need.

Several characterization methods have been used. The optical and electrical properties of the solar cells have been analyzed.

It could be observed that the nanostructured solar cells show a distinctively reduced reflection compared to planar solar cells. The solar cells with the shortest nanowires show the best antireflective behaviour in the visible range while the solar cell with the longest nanowires showed the best antireflection in the near infrared range. The external quantum efficiency (EQE) has been higher for the nanostructured solar cells over a wide range of the spectrum. The solar cell with the shortest nanowires (50 nm high and 670 nm in diameter nanowires) achieved 92% external quantum efficiency (@480nm). Looking at the IV measurements the nanostructured solar cells show slightly higher short circuit current density (J_{SC}) ($31 - 33 \frac{mA}{cm^2}$) than planar cells ($29 \frac{mA}{cm^2}$).

The solar cell achieving the highest efficiency of 11.9% was the nanostructured cell with the longest silicon nano wires ($SiNW$) (500 nm high and 500 nm in diameter).

Kurzfassung

Solarenergie stellt eine gute Alternative zur konventionellen Energieerzeugung dar. Sie ist umweltfreundlich und nachhaltig. Der Markt basiert momentan noch sehr auf kristalline Solarzellen. Hybride Solarzellen vereinen die Vorteile aus der kristallinen und organischen Welt. Der Nachteil sind niedrigere Effizienzen im Vergleich zu kristallinen Solarzellen.

Das Ziel dieser Masterarbeit war die Herstellung von nanostrukturierten hybriden Solarzellen. Nanostrukturen in hybriden Solarzellen könnten die Effizienzen steigern. Es wurde analysiert wie sich verschiedenen Nanodrahtdimensionen auf das Verhalten von Solarzellen auswirken. Diese Nanostrukturen wurden in einem Top-Down Prozess hergestellt der im Zuge dieser Arbeit optimiert wurde. Das Verfahren kann einfach angepasst werden um verschiedene Nanostrukturen herzustellen.

Es wurden verschiedene Charakterisierungsmethoden verwendet. Die Zellen wurden sowohl auf ihre optischen Eigenschaften, als auch auf ihre elektronischen Eigenschaften hin untersucht.

Die nanostrukturierten Solarzellen zeigten eine stark reduzierte Reflektivität im Vergleich zu den planaren Solarzellen. Solarzellen mit den kleinsten Nanodrähten (50 nm hoch, 670 nm Durchmesser) wiesen das beste Antirefleksionsverhalten im VIS Bereich auf während die Solarzellen mit den höchsten Nanodrähten (500 nm hoch, 500 nm Durchmesser) die geringste Reflexion im NIR Bereich aufzeigten. Im Vergleich der externen Quanteneffizienz zeigten die strukturierten Zellen über weite Teile des Spektrums eine höhere Quantenausbeute als die planaren Zellen. Die Solarzelle mit den kleinsten Nanodrähten zeigte bei 480 nm 92% Quantenausbeute. In den IV Messungen zeigten die nanostrukturierten Zellen leicht höhere Leerlaufspannungen ($31 - 33 \frac{mV}{cm^2}$) als planare Solarzellen ($29 \frac{mV}{cm^2}$).

Die höchste Effizienz im Zuge dieser Arbeit wurde von einer nanostrukturierten Solarzelle erzielt und lag bei 11.9%.

Contents

Affidavit	ii
Acknowledgement	iii
Abstract	iv
Kurzfassung	v
1 Motivation	1
2 Basics	3
2.1 Solar cells	3
2.2 Hybrid solar cells	5
2.2.1 Basic design	5
2.2.2 Working principle	7
2.2.3 Nanostructuring	7
2.2.4 Spin coating	8
2.3 Characterization methods	8
2.3.1 Spectrometry	8
2.3.2 IV characterization	9
2.3.3 <i>EQE</i> measurements	13
3 Experimental	14
3.1 Fabrication processes	15
3.1.1 Substrate material	15
3.1.2 Hydroplaning	15
3.1.3 Sphere shrinking	16
3.1.4 Reactive ion etching	17
3.1.5 Lithographing methods	18

3.1.6	Spin coating	18
3.1.7	Front and back contacts	19
3.2	Characterization methods	20
3.2.1	Spectrometry	20
3.2.2	IV characterization	20
3.2.3	<i>EQE</i> measurements	21
4	Results and discussion	22
4.1	Nanostructuring	22
4.1.1	Spin coating	25
4.1.2	Finished solar cell	26
4.2	Optical properties of the structure	27
4.3	Spectral response of the device	32
4.4	IV characteristics of the device	35
5	Conclusion and outlook	38
	List of Figures	40
	List of Tables	42
	Glossary	43
	Bibliography	44

Chapter 1

Motivation

Nowadays crystalline solar cells are commonly used in solar modules. With 25.6% efficiency^[11] (in research) the crystalline solar cells highly out-range organic solar cells that achieve a maximum efficiency of 13.2% efficiency^[7] (in research). Of course this grade of efficiency has its price, as thick layer devices are needed to get the maximum absorption. Therefore large amounts of highly pure silicon are needed which increase the price. The advantages of organic solar cells are numerous despite the low efficiency. As mostly much less material is needed the material costs in overall are low. The material can be processed in cost efficient ways and even be used on flexible foils.

In hybrid solar cells the advantages of inorganic crystalline cells and organic cells are combined. In this study poly(3,4-ethylenedioxythiophene):poly(styrenesulfonate) (*PEDOT:PSS*) was used as the organic part of the hybrid solar cell. The great electric properties and high stability of the crystalline materials are joined with the good absorbance and flexibility of the organic polymer.

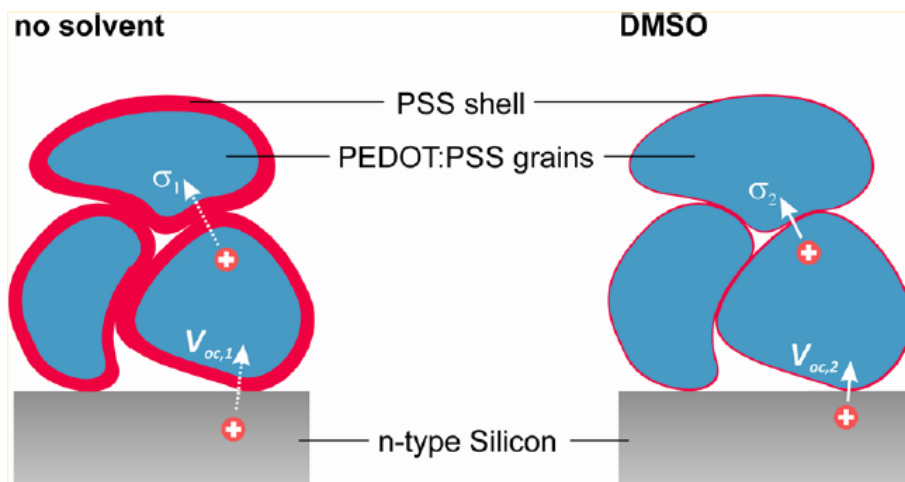


Figure 1.1: Schematic showing the influence of dimethyl sulfoxide (*DMSO*) on *PEDOT:PSS*^[27]

A few micrometer thin *PEDOT:PSS* layer is deposited on top of n-doped silicon (*Si*).

In this work spin coating was used to deposit the PEDOT:PSS. It was important, that the organic material completely coats the nanostructures. By varying the spin coating parameters, a complete coating was achieved. The efficiency of a solar cell using PEDOT:PSS is limited by the charge carrier transport in the PEDOT:PSS layer. This limitation results from the insulating PSS shell that surrounds the *PEDOT:PSS*. By adding *DMSO* to the *PEDOT:PSS* this insulating layer will decrease in thickness and so increases the conductivity (see figure 1.1).

Nanostructures become more and more important in hybrid solar cells. They increase the surface area and simultaneously function as antireflective coating.

In planar solar cells thick layers of highly pure silicon have to be used in order to absorb most of the incoming light while providing a long minority charge carrier diffusion length (L_n) to avoid recombination losses. Using highly pure and crystalline silicon increases the costs of solar cells highly.

Therefore, *SiNW* can be a cheap replacement. The nanowires will enhance the absorption of light^[29] while reducing material costs as they can be fabricated on a glass substrate. Radial pn junction (see figure 1.3) can further reduce the recombination losses as the minority charge carrier diffusion length just has to be half of the nanowire diameter.

In this work *SiNW* are referred as structures with an aspect ratio (length/diameter) of 1-5. Only radial pn junctions have been fabricated. The fabrication of *SiNW* can be done via bottom-up (eg. using chemical vapor deposition (*CVD*)) or top-down methods. This work focuses on top down processes such as reactive ion etching (*RIE*).

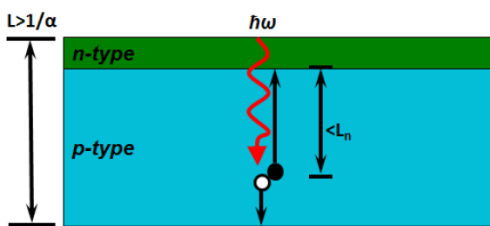


Figure 1.2: Schematic of planar solar cell. The cell thickness L has to be larger than its optical thickness $\frac{1}{\alpha}$ [13]

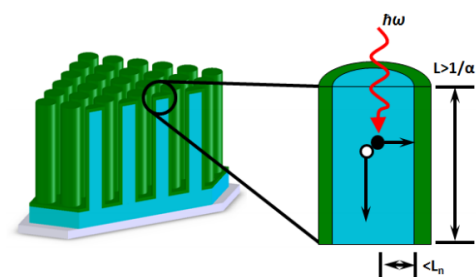


Figure 1.3: Schematic of radial pn junction [13]

Chapter 2

Basics

2.1 Solar cells

A solar cell is a device converting sunlight into electricity using the photovoltaic effect. Basically a three step process is necessary to produce electricity out of light.

- Absorption of sunlight creating an exciton
- Separation of charge carriers
- Extraction of carriers to external circuit

The absorption process is mostly enhanced by different kinds of antireflective coating or a special surface structuring. The more light is absorbed in the cell the more energy can be converted. In the next step the chosen semiconducting material is essential to create as many excitons possible. Therefore the electron is enhanced from the valence band into to the conduction band leaving a hole. This electron-hole pair is called exciton. Now these charges have to be separated from each other. Commonly this is achieved with a p-n junction made out of doped silicon. This p-n junction only works properly with appropriate contacts connecting the device to a terminal where the charge carriers can be extracted to.

There are different forms of solar cells achieving year to year higher efficiencies (see figure 2.1).

- Crystalline silicon solar cells are the most common nowadays. They are the most efficient solar cells on the market. Mono-crystalline silicon solar cells achieve efficiencies of 25.6% (lab report)^[11].
- In thin film solar cells a huge variety of materials are used. GaAs thin film solar cells achieve unrivaled efficiencies of 28.8%^[23].

2.1. SOLAR CELLS

- Multijunction solar cells use combinations of several thin films and combine different semiconducting materials. Triple junction metamorphic cells reach efficiency of 44%^[16].
- Organic solar cells are the newest technology. They achieve maximum efficiencies of 13.2%^[7].
- In hybrid solar cells the advantages of organic and inorganic semiconductors are combined. These solar cells have efficiencies of 13%^[25].

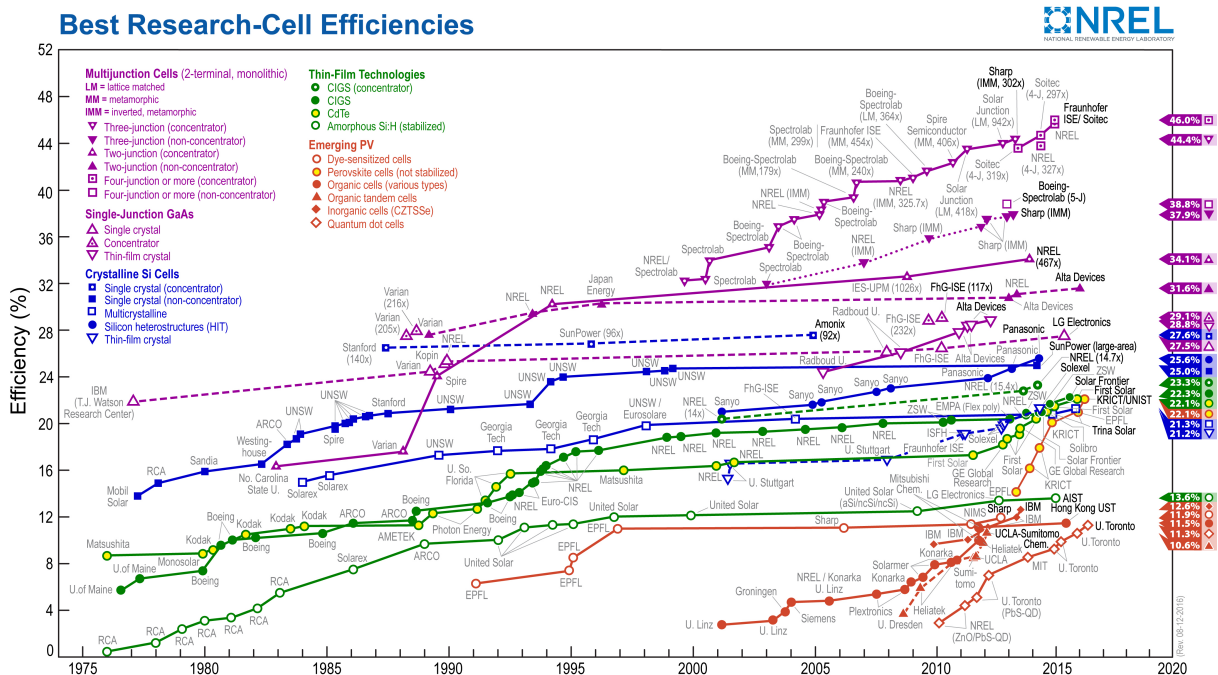


Figure 2.1: Efficiency chart of the best research cell efficiencies reported by NREL^[4]

2.2 Hybrid solar cells

In hybrid solar cells organic and inorganic semiconductors are used together. As organic semiconductors can't be doped in either way there is no p-n junction at the interface but rather a donor-acceptor junction acting as a potential barrier. These two parts have different electron affinities^[10].

The organic polymer acts as the donor material transporting holes while the inorganic semiconductor is the acceptor part and transports the holes. In hybrid solar cells the necessary energy for the charge carrier separation comes directly from the energy offset of the LUMO levels or the conduction bands (see figure 2.2). Basically it can be said that the incoming light generates in exciton in the donor-acceptor junction. The electrons are put up into the conduction band and transported thru the inorganic part of the junction. Whereas the holes are transported by the organic polymer part of the solar cell.

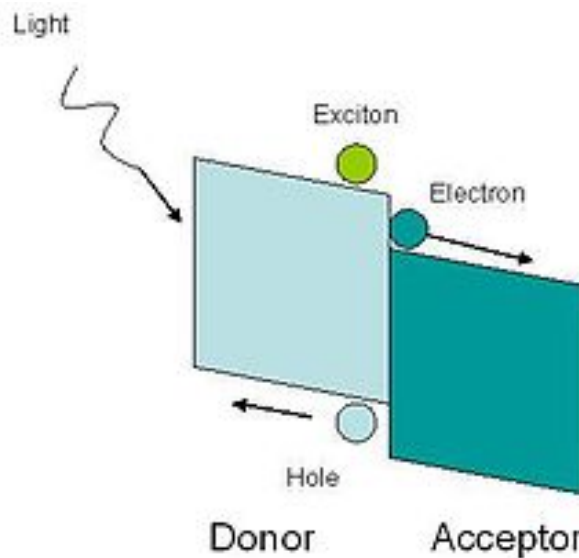


Figure 2.2: Schematic energy diagram of the donor-acceptor interface^[5]

2.2.1 Basic design

The solar cell that is discussed in this work has a top-anode, bottom-cathode design (see figure 2.3). This structure was designed due to the fact, that most low work function materials, that are necessary for collecting the electrons, oxidize quickly and will cause the solar cell to fail. Therefore the cathode was placed on the bottom of the solar cell. Another advantage of this design is that the *PEDOT:PSS* is acidic and can not do any damage to a metal-oxide electrode if it is not contacted directly. In this work a indium gallium

eutectic ($E\text{-In/Ga}$) has been used as a back contact as it can easily be scratched into the back of the n-Si by hand after all the fabrication processes have been completed. The top contact is realized as a gold grid that is evaporated onto the PEDOT:PSS layer. Gold has a high work function (workfunction = 5.1 eV) and does not oxidize. The problem that results from a non-transparent top-anode is the amount of shielding. There are several papers now being published on silver nanowires functioning as transparent electrodes and therefore minimizing the shielding losses of a non-transparent top-electrode^{[31][28]}.

The n-type silicon and the PEDOT:PSS form the donor-acceptor junction in this solar cell.

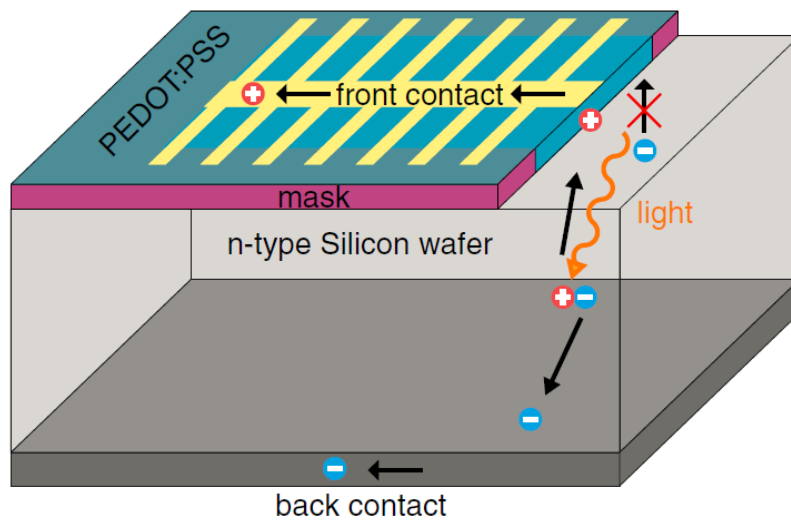


Figure 2.3: Schematic operation scheme of a hybrid solar cell^[24]

2.2.2 Working principle

Light falls onto the surface of the cell. In the depletion region an electron-hole pair is created as the electron moves from the valence band into the conduction band and leaves a vacancy, the hole. This depletion region is created by the donor-acceptor junction formed by the n-Si and the hole conducting *PEDOT:PSS*. In order to obtain a current these generated charges have to be separated before they can recombine. This is done using the built-in electric field that is formed due to the potential difference in the donor-acceptor junction.

2.2.3 Nanostructuring

Nanostructures on the surface of a solar cell have two main effects on its behavior.

1. Antireflective structuring
2. Short transportation distance of the charge carriers to their electrodes.

To reduce light losses due to high reflectivity of planar surfaces nanostructuring helps to minimize the reflectivity. As the charge carriers have short distance to separate, because of the radial donor-acceptor junction, the losses that occur due to recombinations can be reduced. Several papers^[26] have shown, that radial pn junctions can optimize hybrid solar cells. Especially in the wavelength region of 300-600nm high EQE have been measured^[32]. These radial pn junctions are created with *SiNW*. There are different ways of creating *SiNW*. In this work a top down process was performed.

2.2.4 Spin coating

Spin coating is an easy way to control the polymer film that is applied on the substrate. There are two parameters that have been varied: the spin speed (ω) and the spin time (t). Both control the thickness of the deposited film. The spin acceleration ($\frac{d\omega}{dt}$) was not changed in this work. A defined amount of the polymer is deposited on the surface of the substrate (figure 2.4a). During the acceleration a homogeneously thin film is created (figure 2.4b). The spare material is spun off (figure 2.4c) and in the last step the solvent evaporates and leaves a thin polymer film on the substrate.

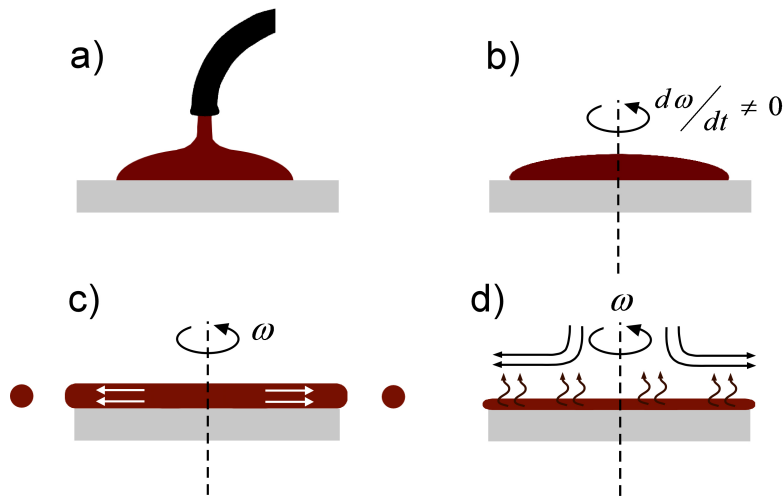


Figure 2.4: Schematic of the different stages of spin coating^[2]

2.3 Characterization methods

2.3.1 Spectrometry

If light hits an object there are basically three things that can happen: reflection, transmission and absorption. A spectrometer is designed that all three outcomes can be measured separately.

For a solar cell it is essential that the reflectivity is cut down to a minimum to get as much light into the region to create an electron hole pair.

The reflectance is the ratio of the reflected and the incident intensity and can also be calculated using equation 2.1.

$$R = \left(\frac{n_a - n_b}{n_a + n_b} \right)^2 \quad (2.1)$$

R [%]	reflection
n_a	refractive index of first medium
n_b	refractive index of second medium

There are two ways to reduce reflection to a minimum: Anti reflective coating and structuring of the surface. In this work both methods have been used. Using anti reflective coating the thickness of this layer as well as its refractive index is relevant. Using equation 2.2 the best refractive for the anti reflective coating can be calculated .

$$n_1 = \sqrt{n_0 n_2} \quad (2.2)$$

n_1	refractive index of the antireflective coating
n_0	refractive index of the surrounding material
n_2	refractive index of the substrate

If the refractive index n_1 of the coating material is set the thickness can be varied to obtain optimum reflection behavior see equation 2.3. The thickness differs for different incident wavelengths.

$$d = \frac{\lambda_0}{4n_1} \quad (2.3)$$

d [nm]	thickness
λ_0 [nm]	incident wavelength

2.3.2 IV characterization

The IV characterization is one of the most powerful methods to evaluate the functionality of a solar cell. There are several values that can be derived from an IV curve: the short circuit current (I_{SC}), the open circuit voltage (V_{OC}) and the fill factor (FF). With these values the efficiency can be derived with equation 2.4.

$$\eta = \frac{V_{OC} I_{SC} FF}{P_{in}} \quad (2.4)$$

2.3. CHARACTERIZATION METHODS

η [%]	efficiency
V_{OC} [V]	open circuit voltage
I_{SC} [A]	short circuit current
FF	fill factor
P_{in} [W]	input power

Using a solar simulator the fabricated cell is illuminated with a calibrated power and the AM 1.5G spectrum. If there is no illumination the solar cell shows a diode characteristic behavior only depicting dark current. The incoming light shifts the IV curve down so power can be generated. In equation 2.5 the IV equation can be seen.

$$I = I_L - I_0 \left(\exp\left(\frac{qV}{nkT}\right) - 1 \right) \quad (2.5)$$

n	ideality factor
$k = 1.38 * 10^{-23} \left[\frac{J}{K} \right]$	Boltzmann constant
T [K]	temperature
I_L [A]	light generated current
I_0 [A]	dark saturation current
$q = 1.6 * 10^{-8} [C]$	elementary charge
V [V]	voltage

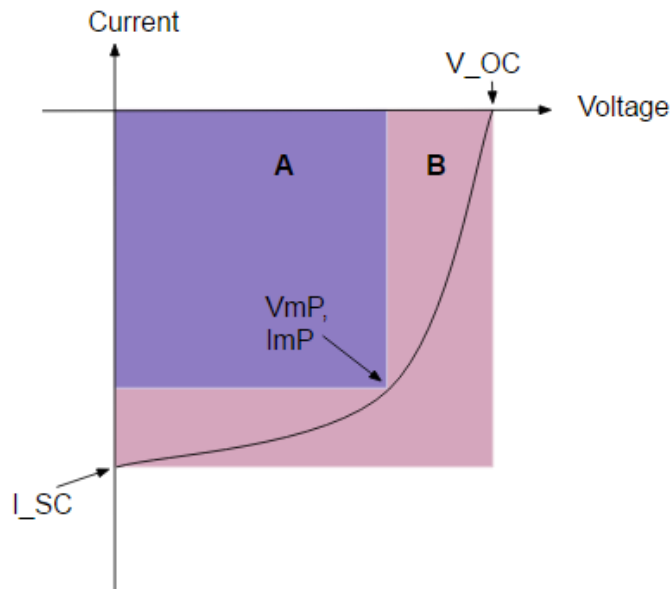


Figure 2.5: Schematic used for the calculation of the FF

The I_{SC} is the maximum current the cell can generate. It is measured when the voltage is zero, mostly due to short circuiting the device. The I_{SC} is dependent on the optical properties of the solar cell as it depends on the absorbed photons as well as on the light spectrum.

2.3. CHARACTERIZATION METHODS

The V_{OC} is the the maximum voltage the solar cell is able to create while zero current is flowing. Looking at equation 2.6 it can be seen, that the V_{OC} not only depends on the light generated current but as well on the dark saturation current which is dependent on the recombinations.

$$V_{OC} = \frac{nkT}{q} \ln\left(\frac{I_L}{I_0} + 1\right) \quad (2.6)$$

The FF is calculated with equation 2.7 the corresponding plot can be seen in figure 2.5. The FF determines the *squareness* of a solar cell. As round edges minimize area A (see figure 2.5) the higher the FF the better the solar cell as it directly influences the efficiency.

$$FF = \frac{V_{mP} I_{mP}}{V_{OC} I_{SC}} = \frac{\text{area}A}{\text{area}B} \quad (2.7)$$

V_{mP} [V] voltage at maximum power point
 I_{mP} [A] current at maximum power point

There are several defects that can produce deviation from an ideal I-V curve. Especially the shunt resistance and the series resistance will affect the shape of the I-V curve. Both can be modeled in an electric circuit as a parallel resistance (R_{Sh}) and serial resistance (R_S) (see figure 2.6).

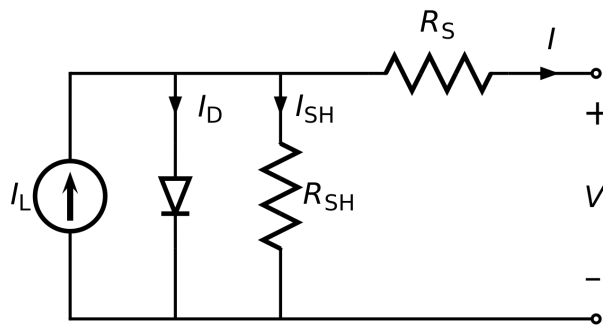


Figure 2.6: Electrical circuit with shunt and series resistance^[6]

In an ideal solar cell the shunt resistance R_{Sh} is infinite. If its not infinity it might provide an alternate path for the current flow and therefore reduce the voltage of the solar cell (see figure 2.7). The value of the R_{Sh} can be estimated from the slope of the IV curve near the short-circuit current point^[21]. The main reason for R_{Sh} is due manufacturing processes that may cause impurities and defects which lead to leakage current.

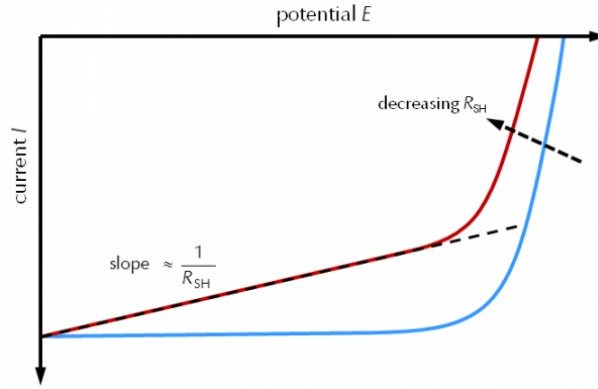


Figure 2.7: Impact of the shunt resistance on the I-V curve^[3]

The series resistance is zero for an ideal solar cell. In a real solar cell the I-V curve is deviated from its ideal form because of it (see figure 2.8). It is mainly caused by the metal electrodes and reduces the fill factor. The main causes are the current resistance of the metal electrodes and the contact resistance. It can be determined by the slope of the I-V curve at the open circuit voltage point^[18].

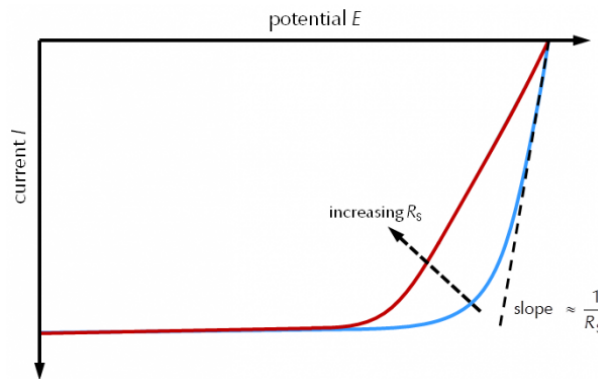


Figure 2.8: Impact of the series resistance on the I-V curve^[3]

2.3.3 *EQE* measurements

The *EQE* is the ratio of all collected charge carriers and all incident photons^[8]. So it is a measure for the ability of the solar cell to convert the incoming light into electricity. As in figure 2.9 can be seen, there are several reasons why a real solar cell will never achieve the perfect square plot of an ideal cell. As short wavelengths such as blue light will not penetrate deep into the cell the main losses result from surface recombinations. At longer wavelengths the diffusion length plays an important role. The diffusion length describes the average distance traveled by charge carriers before recombination. That means if that length is short the probability is very high, that the charges recombine before they can get to the electrode.

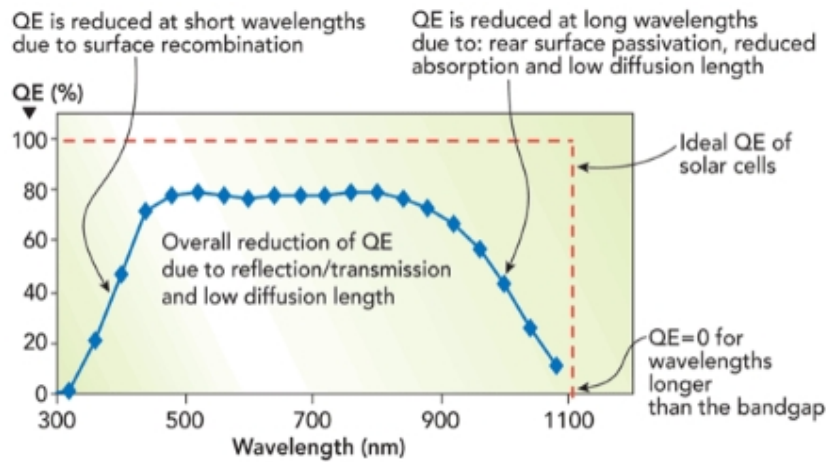


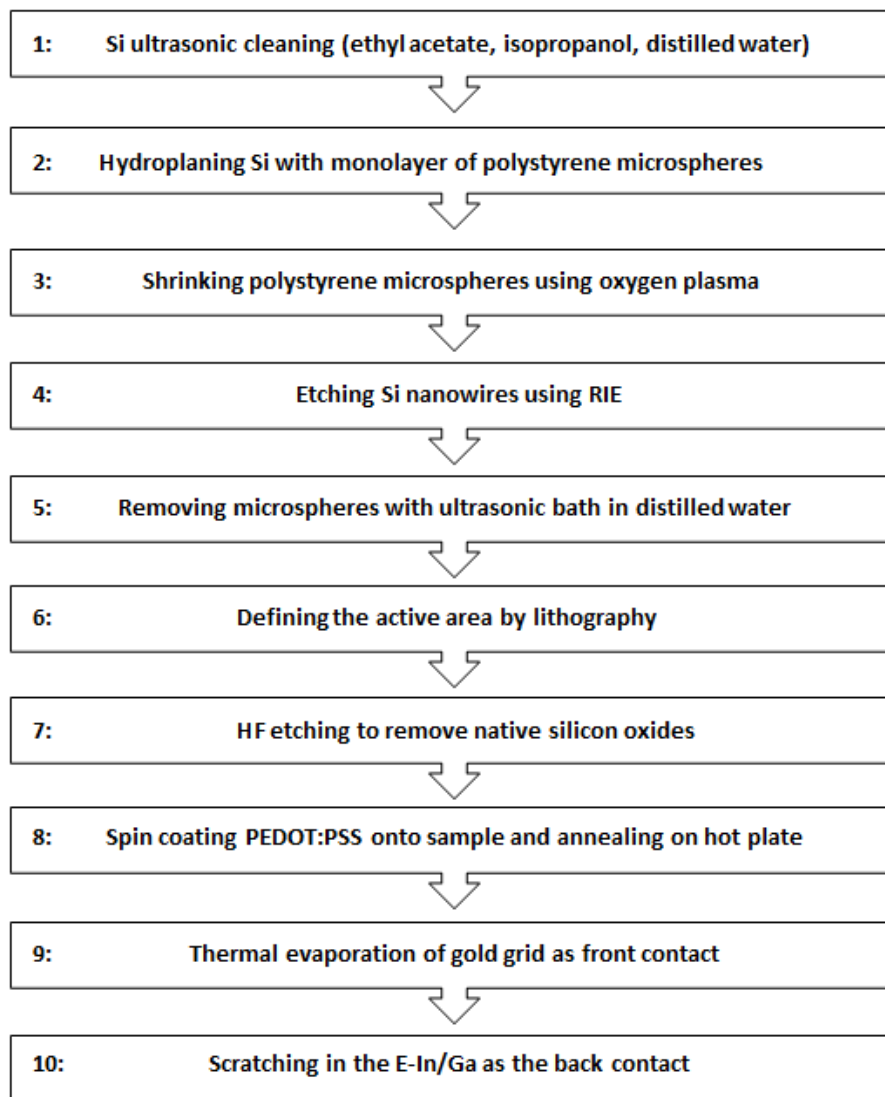
Figure 2.9: Theoretical description of an *EQE* plot, including the main reason for losses^[9]

Chapter 3

Experimental

There are several steps to manufacture the present solar cell. In scheme 3.1 the individual steps can be seen.

These steps are explained in more details, as follows.



Scheme 3.1: Process of manufacturing a hybrid solar cell

3.1 Fabrication processes

3.1.1 Substrate material

A n doped (phosphorus) *Si* wafer with a $1 - 5 \Omega\text{cm}$ resistivity with the $\langle 100 \rangle$ direction facing up was cut into the right size and used as a substrate. The wafer was provided and the doping not changed in any way.

Essential for the functionality of the solar cell is the removal of the native oxide layer that forms if the substrate comes into contact with air. The best method for this cleaning is a hydrogen fluoride (*HF*) dip just before the polymer is deposited on top. A 5% *HF* solution is used. This process will leave the sample hydrophobic.

3.1.2 Hydroplaning

The nanostructuring follows a three step process. First polystyrene microspheres are deposited in a closed packed manner onto a substrate. To get a perfectly arranged monolayer of polystyrene spheres hydroplaning was chosen to be the easiest method^[30]. Polystyrene spheres with an average diameter of $1\mu\text{m}$ are dissolved in water and ethanol is added 1:1 to the solution.

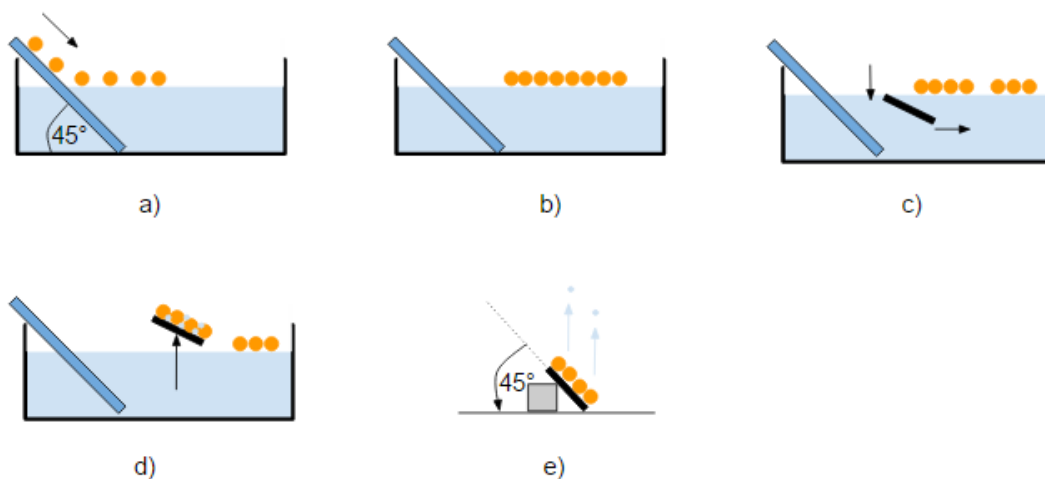


Figure 3.1: Schematic hydroplaning process. a) the spheres are dribbled on the glass slide and onto the water. b) there they form a closepacked monolayer. c) the substrate is placed in the water and underneath the monolayer. d) then it is slowly and slightly tilted pulled out. e) the sample dries in a 45° angle to get rid of the remaining water and solvents

A broad beaker is filled with distilled water and a small amount of sodium dodecyl sulfate (*SDS*) is added to the water to get a concentration of about $0.17 \frac{mmol}{L}$. These *SDS* molecules form a barrier for the microspheres and therefore will help the close packing process^[30]. If there is too much *SDS* in the water the chances are high that the spheres will form multilayers as they will tumble over each other because the barrier is too strong to be overcome. If there is no *SDS* added the spheres will probably not form a close packed monolayer but just float around in small agglomerations and gaps will form. A microscope slide is cleaned and made hydrophilic via oxygen plasma. The slide is put into the beaker leaning on the edge of it to form a 45° angle (see figure 3.1a).

The polystyrene sphere solution is dribbled drop by drop onto the slide so they will slowly move onto the water surface. There they will form a monolayer. This can be seen by the iridescent colors of the water surface.

The cleaned samples are attached to a piece of *Si* wafer using double sided adhesive copper tape. Holding the wafer with tweezers the sample is dipped into the water and while slightly tilting it pulling it out (see figure 3.1d). The dazzling colors now can be seen on the surface of sample. It is left in 45° angle to dry.

3.1.3 Sphere shrinking

In the second step these microspheres are shrunk using oxygen plasma. The plasma cleaner can be used to shrink the polystyrene spheres in diameter. The oxygen plasma will bombard the microspheres from the top and so remove some of the polystyrene. As this process is highly anisotropic the spheres are most affected on the top than on the sides. The plasma cleaner can be used to shrink the polystyrene spheres in diameter. The sample is placed inside the chamber which is evacuated up to 0.2 mbar. Then the oxygen is regulated that the inner pressure reaches a constant 0.4 mbar. Now the plasma can be ignited. The oxygen plasma will bombard the nanospheres from the top and so remove some of the polystyrene.

3.1.4 Reactive ion etching

As described before reactive ion etching is a good method to create *Si* nanostructures. After that the substrate is etched with a *RIE*. *RIE* parameter can be controlled very well and is therefore chosen as the etching method. As a source gas sulfur hexafluoride (SF_6) is used because the fluoride radicals, that are separated before, bond with the *Si* to form SiF_x . This molecule is gaseous and can easily get rid off with a vacuum pump. Since this process is isotropic a surface passivisation is needed. For that reason the chamber is cooled with liquid nitrogen down to $-110\text{ }^\circ\text{C}$ ^[20]. All etching parameters, expect the etching time have not been changed during this work (see table 3.1). These parameters are experience values already provided for me.

The *Si* substrate with the deposited and shrunk microspheres on top is fixed on a carrier wafer with a drop of oil. To avoid any residues or unsatisfactory performance of the process the oil must not ooze out under the substrate. The carrier wafer with the perfectly attached substrate on top are placed into the chamber which is then evacuated and the etching process is performed fully automatically. After the etching is complete the substrate is removed from the carrier wafer and dipped for 60 s in distilled water in the ultrasonic bath in order to get rid of the remaining polystyrene spheres. The nanospheres that are still resting on the top of the *SiNW* are easily be removed if the sample is dipped for 60 s in distilled water in the ultrasonic bath.

Table 3.1: *RIE* operating parameters used in the experiments

Pressure [mtorr]	O_2 flow [sccm]	SF_6 flow [sccm]	ICP [W]	RF [W]	Temperature [$^\circ\text{C}$]
7.0	8.0	40.0	475.0	6.0	-110

3.1.5 Lithographing methods

In order to have a defined active area of the solar cell a photoresist mask is applied on the nanostructured surface using the *Karl Suss* mask aligner (see figure 3.2). The AZ nLOF 2070 negative photoresist is used in a $(3.5 \pm 0.2) \mu\text{m}$ thick layer. This photoresist shields the layers below from light contact and therefore electron hole pair generation.

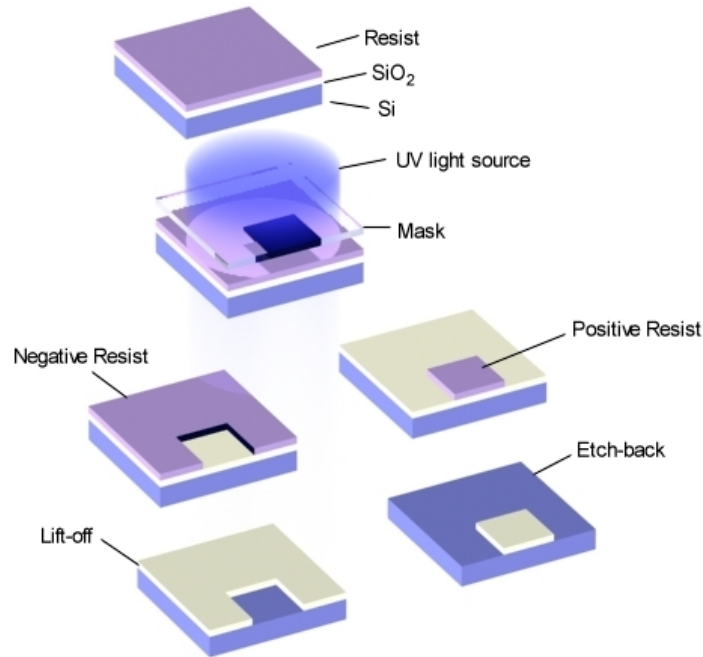


Figure 3.2: Basic working principle of a lithographing process^[17]

3.1.6 Spin coating

The polymer used in this work is *PEDOT:PSS*. As the PSS will form an insulating shell around the *PEDOT:PSS* grains adding *DMSO* will reduce the shell thickness and so enhance the conductivity of the polymer. In order to get a distribution of the solution a wetting agent is added. The exact recipe of the solution was determined experimentally and already provided for me and can be found in table 3.2. To avoid insulation coming from the native oxides of the *Si* substrate itself the sample is dipped into *HF* for 60 s before spin coating it.

The spin coating parameters have been optimized in a way that the polymer coats the *SiNW* from top to bottom.

The resulting spin parameter can be found in table 3.3.

Table 3.2: Composition of the polymer solution used in the experiments

Sample	Ratio PEDOT:PSS : DMSO : Wetting Agent
Nanostructured sample	1000:50:10,5
Planar sample	1000:50:1

Table 3.3: Spin parameter used in the experiments

Spin speed [rpm]	Acceleration [$\frac{rpm}{sec}$]	Spin time [sec]
8000	15	60

3.1.7 Front and back contacts

A gold grid is applied via evaporation to function as the front contact. A *E-In/Ga* is scratched into the back of the solar cell to work as the back contact.

3.2 Characterization methods

3.2.1 Spectrometry

The reflectivity is measured using the spectrophotometer *Cary5000* from *Varian* (see figure 3.3). Only reflectivity measurements have been performed with the incident beam hitting the sample at a 90° angle. The reflected light is measured with an integrating sphere.



Figure 3.3: Spectrophotometer

3.2.2 IV characterization

To measure the IV curve the solar simulator *Sol 3A* from *Newport* is used (see figure 3.4). The AM 1.5G spectrum has been used for all measurements.



Figure 3.4: Solar simulator

3.2.3 *EQE* measurements

The EQE measurements have been performed with the *Quantum Efficiency Measurement System* from *Newport* (see figure 3.5).



Figure 3.5: EQE measurement system^[12]

Chapter 4

Results and discussion

4.1 Nanostructuring

During the hydroplaning process it is essential to tilt the sample while the substrate is pulled out of the beaker. If the sample is not tilted but held horizontally too much water will remain on the surface and while drying slide some spheres over each other. This can be seen with the naked eye as drying *lines* will form multilayer lines (see mark B in figure 4.1) and individual spheres might rest on the monolayer below (see mark A in figure 4.1).

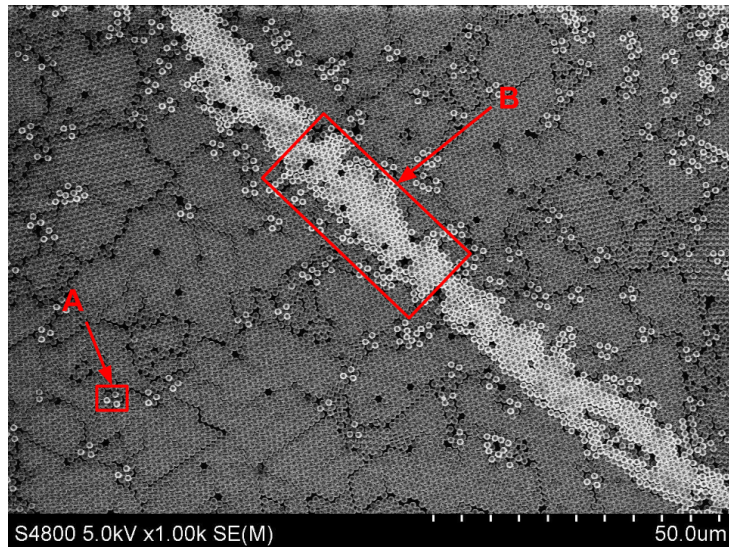


Figure 4.1: Too much water on the surface might form multilayer *lines* as seen in the scanning electron microscope (*SEM*)

After the hydroplaning closed packed monolayers of polystyrene spheres cover the surface of the substrate. This monolayers behave like crystal structures and form out crystal defects such as point defects (eg. vacancies see figure 4.2 A) or line defects (eg. edge dislocations see figure 4.2 B).

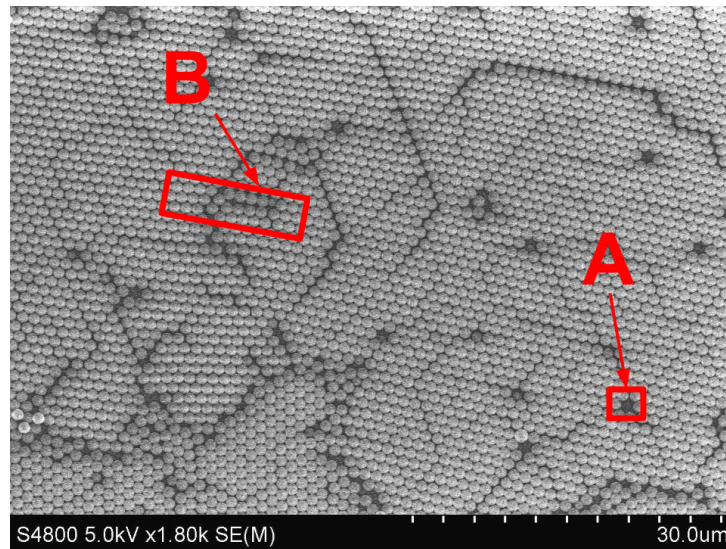


Figure 4.2: *SEM* image of a monolayer of polystyrene spheres pointing out defects in the structure

These microspheres are shrunk using oxygen plasma. The shrink rate of the diameter behaves nicely linear regarding the plasma etching time (see figure 4.3).

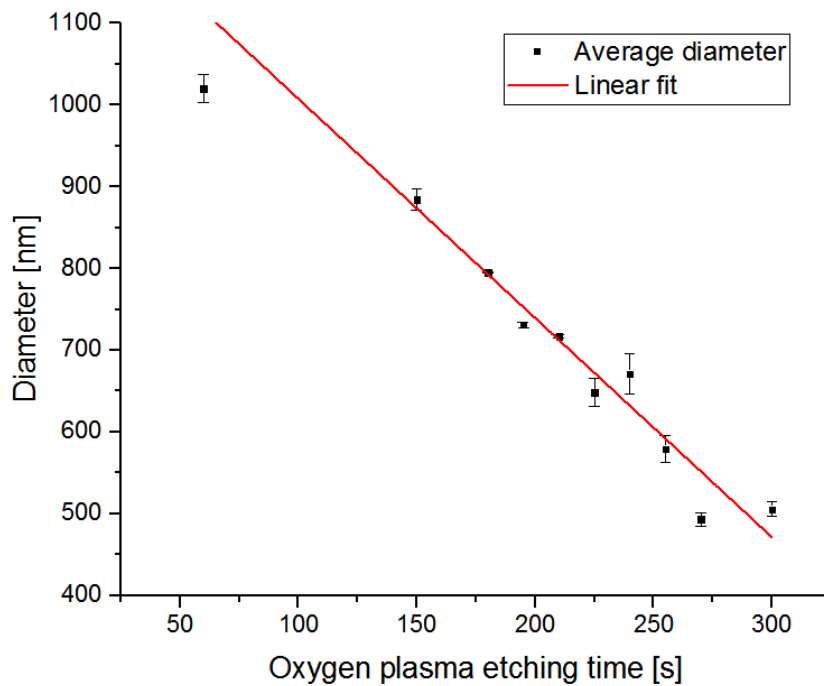


Figure 4.3: Average diameter as a function of etching time measured in a *SEM*

Using a *SEM* it can be seen that the spheres have a lentil-like shape at the end of the shrinking process (see figure 4.4). This can be explained as the oxygen plasma will not affect the spheres isotropically but rather more on the top than on the sides.

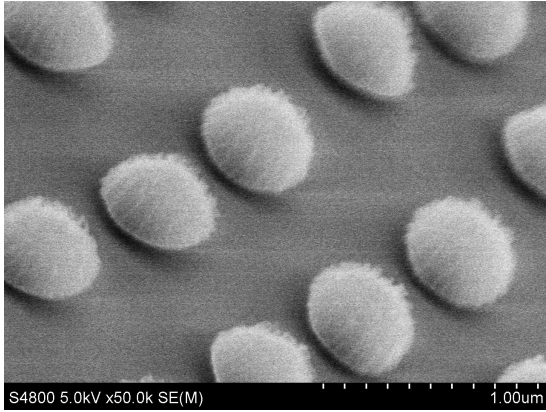


Figure 4.4: image of the lentil-like shape of microspheres shrunk in oxygen plasma

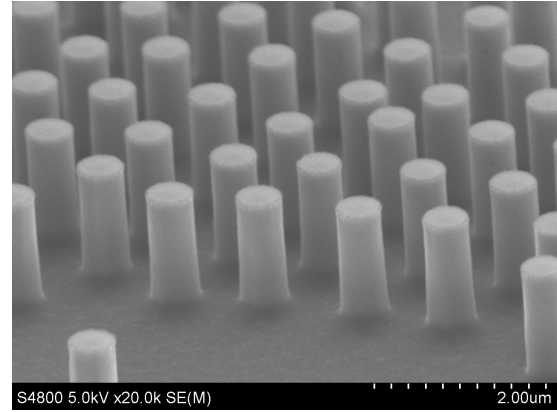


Figure 4.5: SEM image of the *SiNW* after the nanospheres have been washed away

After the shrinking process the real nanostructuring process is performed using a *RIE*. As the etching process was performed under low temperatures ($-110\text{ }^{\circ}\text{C}$) the chemical isotropic reaction of the etching is slowed down so that the *SiNW* surface is smooth and straight (see figure 4.5). The little roughness that is still remaining can be removed with a *HF* dip. The height of the *SiNW* behaves linear to the etch time (see figure 4.6).

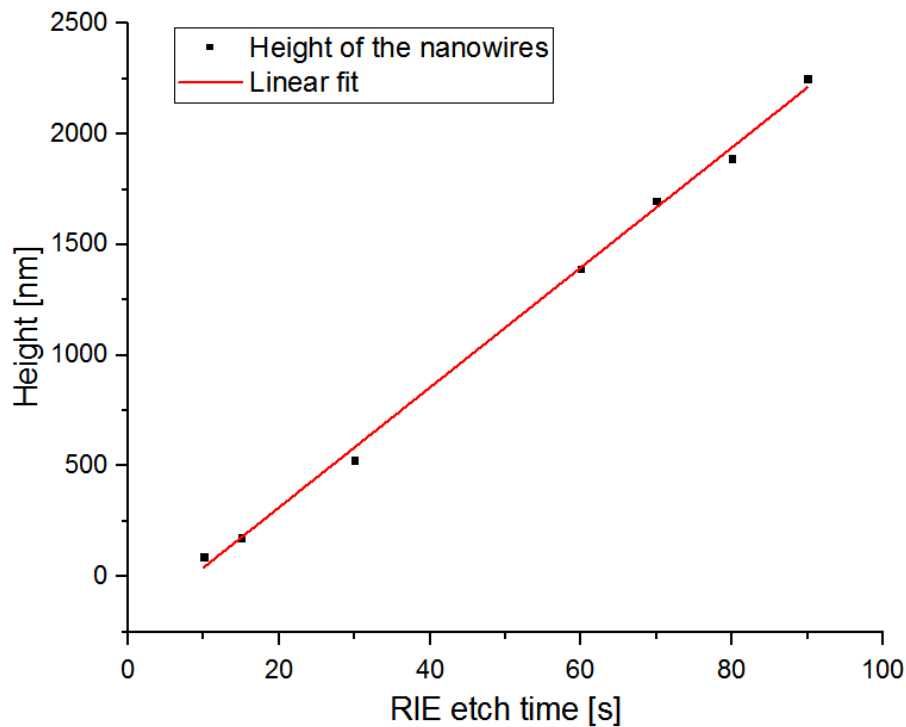


Figure 4.6: Linear behavior of the height of the *SiNW* considering the reactive ion etch time

4.1.1 Spin coating

In figure 4.7 a sample is shown consisting of an area with perfectly coated *SiNW* (area B) and another area with the polymer only *hanging* between the *SiNW* without touching the bottom (area A). If the solar cells are produced with the polymer only partly covering the *SiNW* it is impossible to tell whether they arise from the insufficient coverage or other reasons.

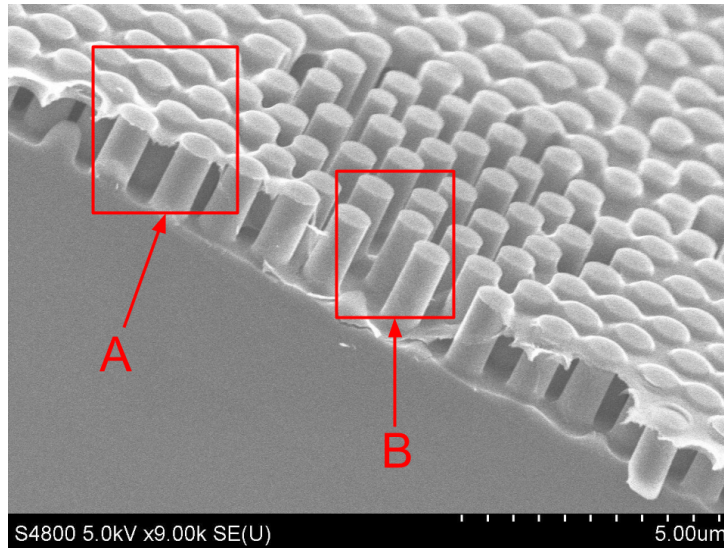


Figure 4.7: *SEM* cross section image of a nanostructured sample coated with *PEDOT:PSS*

4.1.2 Finished solar cell

The finished solar cell can be seen in figure 4.8. There the nanostructures can be seen as the surface of the cell shows iridescent colors. It can be seen in figure 4.9 that the back contact does not cover the back of the solar cell homogeneously.

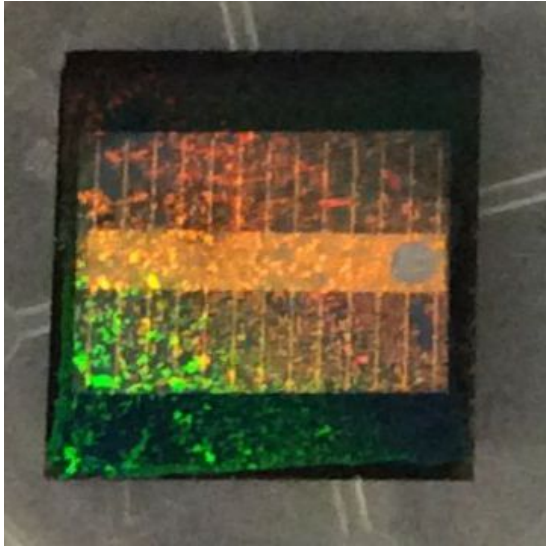


Figure 4.8: Photography of the front contact of a solar cell with nanostructures

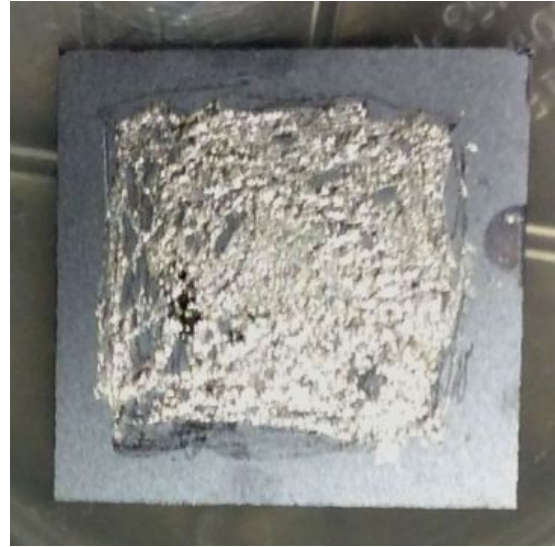


Figure 4.9: Photography of the back contact of a finished solar cell

4.2 Optical properties of the structure

To reduce the optical losses at illumination of a solar cell its surface interface reflectivity should be minimized. Using a spectrometer the reflectivity of nanostructured samples and finished solar cells has been measured.

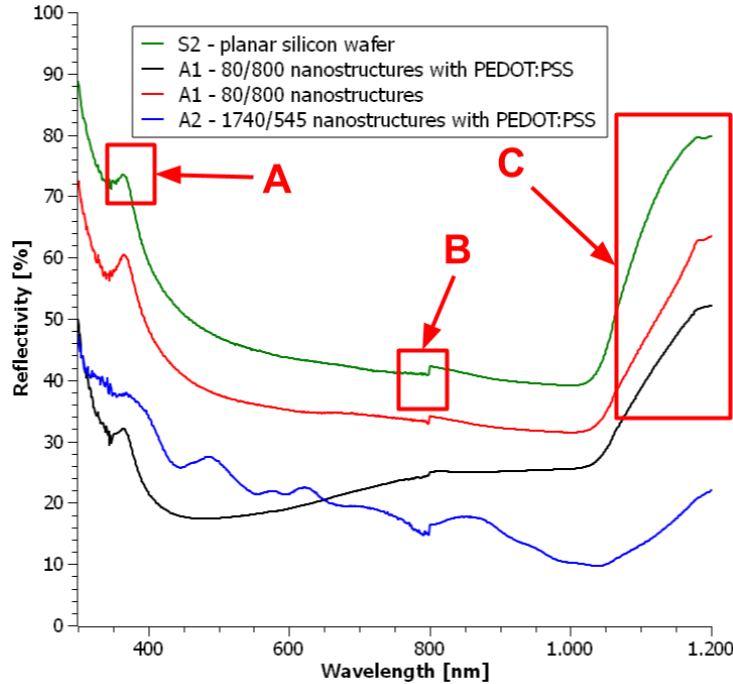


Figure 4.10: Reflectivity spectra of differently nanostructured *Si* wafer with and without *PEDOT:PSS* coating

In figure 4.10 the reflectivity of three differently manufactured samples are compared to that of a planar *Si* wafer.

The peak marked with "A" results from the high refractive index of *Si* at that point (n_{Si} @370 nm = 6.863). This peak can be seen in all measurements as all samples have a silicon substrate.

The sharp edge that is seen at wavelength 800 nm (marked with a "B") results from the change of lamps in the measuring spectrometer. As *Si* has a band gap of 1.11eV there is a sharp drop in the absorption coefficient of *Si* @1100 nm. Low absorption coefficients mean that the light is poorly absorbed therefore the reflectivity increases (marked with a "C") as the sample is too thick to transmit light.

As almost 85%^[19] of the irradiance of the solar spectrum lies between 300 nm - 900 nm the incoming sunlight with wavelengths above 900 nm will not contribute an essential part to the solar cell input. It makes more sense to optimize a solar cell in a wavelength

4.2. OPTICAL PROPERTIES OF THE STRUCTURE

range with a high irradiance than in one with low irradiances.

It can be seen that sample A1, without PEDOT:PSS coating acts almost like the planar *Si* wafer (S2) but showing less reflectivity. As the reflectivity curve of the A1 sample is just shifted down a bit, compared to the curve of the planar silicon wafer it can be said, that the tiny nanostructures (*80 nm height and 800 nm in diameter*) result in reduced reflectivity. This might result from the tiny *SiNW* height. As they are much smaller than the incident wavelengths the surface acts like having a continuous refractive index gradient. As the plain air-*Si* interface is removed that way the reflections are reduced.

If that nanostructures are coated with PEDOT:PSS the reflectivity is minimized even further (see curve of sample A1 after PEDOT:PSS coating). It is not really understood why this measurements show a slight increase of reflectivity between 450 nm – 800 nm.

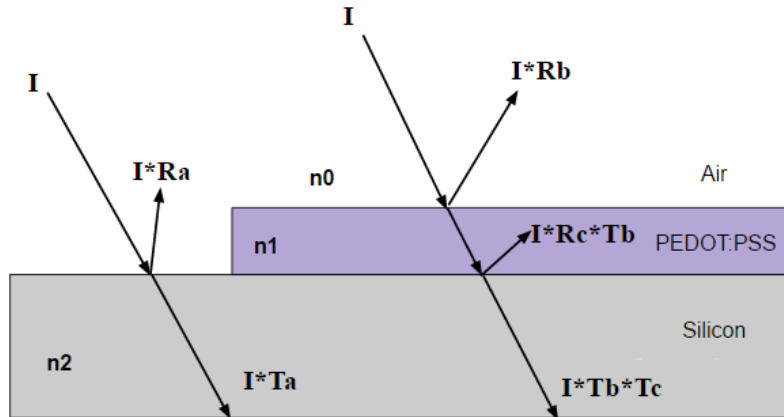


Figure 4.11: Multiple reflections between air, *PEDOT:PSS* and *Si* reducing the total reflectivity

n_0	refractive index of air
n_1	refractive index of PEDOT:PSS
n_2	refractive index of silicon
I	Intensity of the incident light
$R_a[\%]$	reflectivity at the silicon-air interface
$R_b[\%]$	reflectivity at the PEDOT:PSS-air interface
$R_c[\%]$	reflectivity at the Silicon-PEDOT:PSS interface
$T_a[\%]$	transmittance of light from air into silicon
$T_b[\%]$	transmittance of light from air into PEDOT:PSS
$T_c[\%]$	transmittance of light from PEDOT:PSS into silicon

If light enters the *Si* without any additional layer the reflectivity is $R_a = 35\%$, giving a maximum transmittance of $T_a = 65\%$ (with $n_2 = 3.9 @600 \text{ nm}^{[15]}$).

4.2. OPTICAL PROPERTIES OF THE STRUCTURE

$$T = 1 - (A + R) \quad (4.1)$$

T [%] Transmittance
A [%] Absorbance
R [%] Reflectance

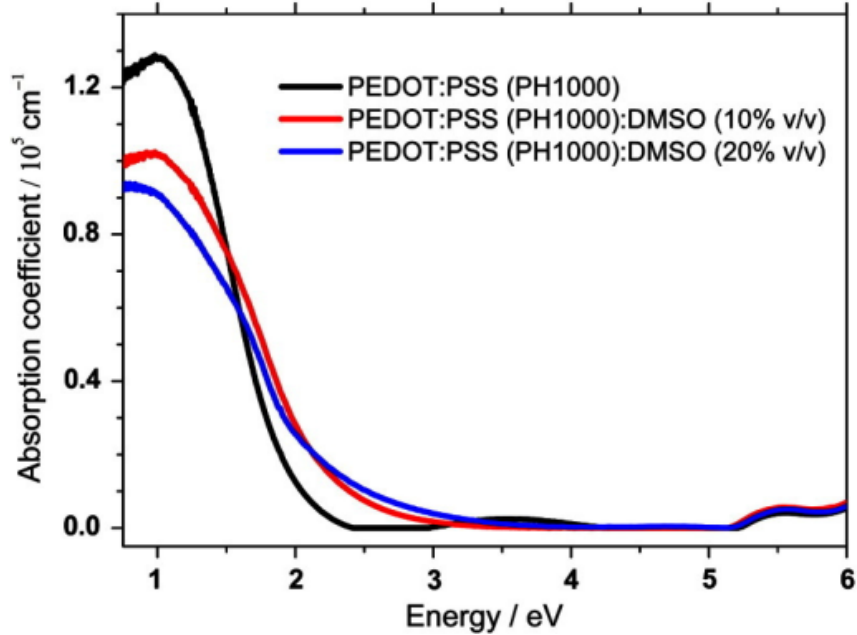


Figure 4.12: Absorption coefficient of PEDOT:PSS:DMSO^[22]

In figure 4.12 the absorption coefficient of PEDOT:PSS with DMSO can be seen. The mixture used in this work has a lower DMSO concentration (4.7%) than the concentrations mapped in figure 4.12, but it can be assumed that it is just below the curves with 10% DMSO concentration. At 400 nm the absorption coefficient is about $0.1 * 10^5 \text{ cm}^{-1}$. This means that the absorption depth at 600 nm is about $1 \mu\text{m}$. The absorption depth describes the distance in a material where the light has lost 36% of its intensity^[1]. As the polymer layer thickness is between $50 \text{ nm} - 80 \text{ nm}$ only a very small part of the intensity of the light is lost due to absorption. The absorption depth of PEDOT:PSS with DMSO increases even further as the wavelengths increase. Due to that reason the absorption is neglected in the following calculations.

4.2. OPTICAL PROPERTIES OF THE STRUCTURE

If a thin *PEDOT:PSS* layer is deposited on the silicon the entering light is reflected at the air-*PEDOT:PSS* interface (R_b) and at the *PEDOT:PSS-Si* interface (R_c). The total transmittance through both layers is given in equation 4.2.

$$T_{total} = T_b * T_c \quad (4.2)$$

This gives a $T_{total} = 75\%$ (with $n_1 = 1.4 @600 \text{ nm}^{[14]}$).

So it can be said, that by adding a layer of *PEDOT:PSS* the reflectivity is reduced by 10% as more light is transmitted into the *Si* layer. As said above, of course there is light absorbed in the *PEDOT:PSS* layer. But as the absorption depth is much higher (for wavelengths bigger than 400 nm) than the layer thickness the absorption was neglected in this calculation.

If the height of the *SiNW* is increased to an aspect ratio higher than 1.5 resonance behavior can be observed in the reflectivity measurements (see curvy-like patterns in figure 4.10 of sample A2). This can be seen at the reflectivity of the sample *A2* which has an aspect ratio of about 3.1 (1740 nm height and 545 nm in diameter). If the *SiNW* are short they are not able to resonate with the incident light as the waves penetrate deep into the *Si* (see figure 4.13). The entering angle of the reflectivity measurements has been 90° to the surface of the sample.

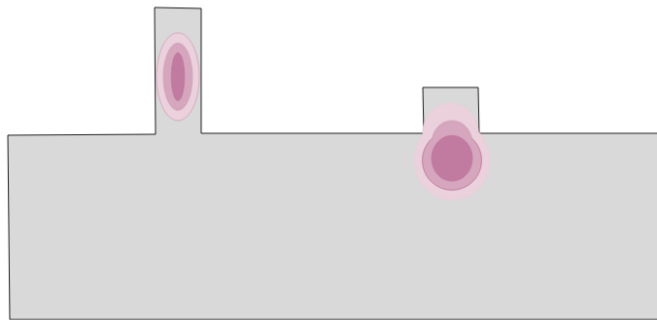


Figure 4.13: Schematic resonance behavior of long *SiNW* and light coupled deep into the *Si*.

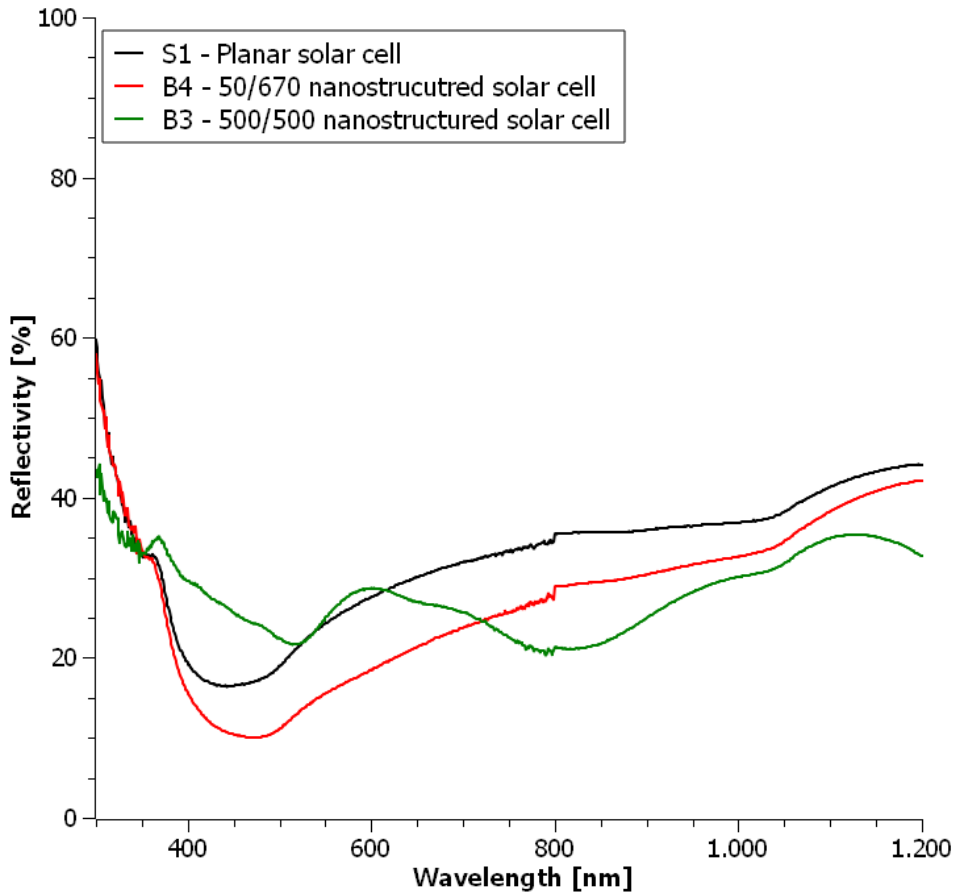


Figure 4.14: Reflectivity spectra of differently nanostructured solar cells compared to a planar solar cell

In figure 4.14 different reflectivity spectra of finished solar cells can be seen. As measurements have shown (see figure 4.10) samples with very tiny nanostructures, such as B4 (50 nm height and 670 nm in diameter), behave the same way planar samples (S1, planar solar cell) do but with much better antireflective behavior. Especially in the visible range this solar cell (B4) shows the lowest reflectivity measurements.

The solar cell with high nanowires B3 (500 nm height and 500 nm in diameter) show the lowest reflectivity measurements in the near infrared range. Due to their nanowire length clear resonance behavior can be seen.

4.3 Spectral response of the device

All photons with energies smaller than the band gap will not create an electron hole pair. Therefore the EQE is 0% for wavelengths larger than 1100 nm.

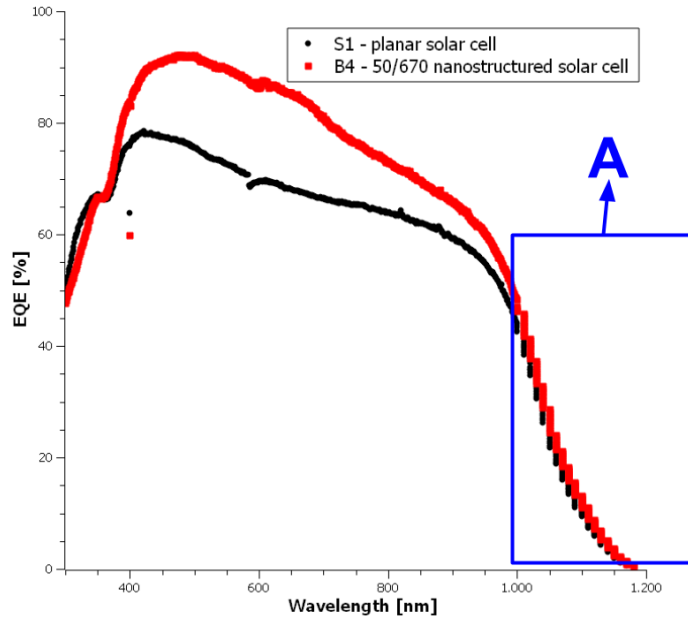


Figure 4.15: EQE spectra of a planar solar cell compared to a nanostructured solar cell with tiny $SiNW$

It can be seen in figure 4.15 that the nanostructured solar cell B4 (50 nm height and 670 nm in diameter) shows much higher EQE than the planar solar cell S1. This is a result of a better incoupling of light (see reflectivity measurements above) and the much larger organic-inorganic semiconductor interface (because of the nanostructures). The continuous increase in figure 4.15 at wavelengths 300 nm - 400 nm results from surface recombination as the ultraviolet light does not penetrate deeply into the cell but is absorbed very close to the surface. This can be seen for the measurements of the nanostructured solar cell as well as for the planar one.

Nevertheless solar cell B4 (50 nm height and 670 nm in diameter) shows even higher EQE in the range 400 nm – 950 nm than the planar cell. This probably results from the radial organic-inorganic semiconductor junction which decreases the necessary diffusion length of the charge carriers and therefore the amount of the recombination losses.

The area marked with an "A" in figure 4.15 results from change of the step size during the measurement.

4.3. SPECTRAL RESPONSE OF THE DEVICE

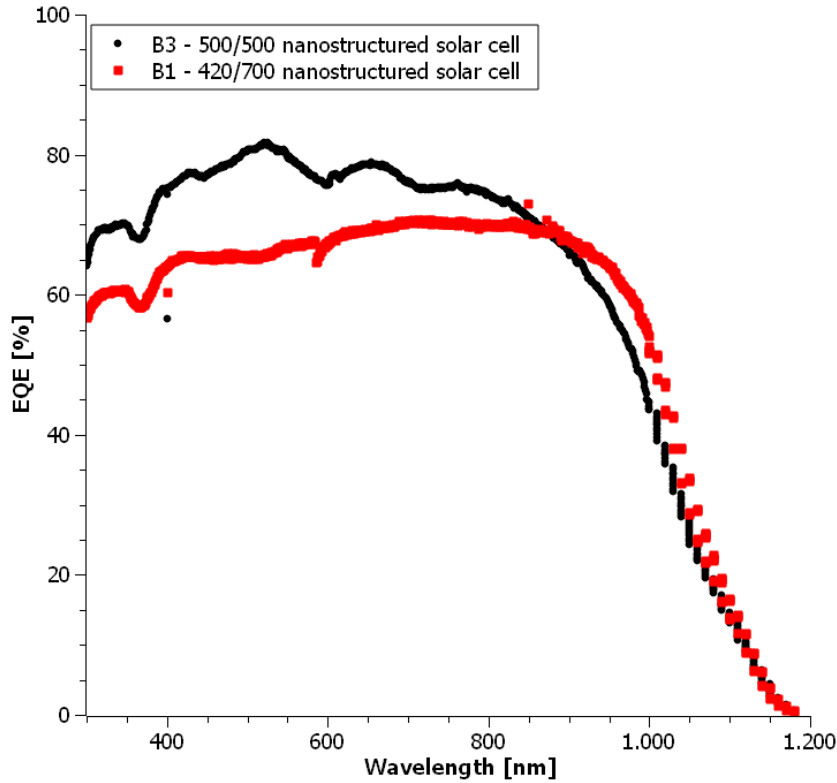


Figure 4.16: *EQE* spectra of two nanostructured solar cells with high *SiNW*

In figure 4.16 it can be seen that solar cell B3 (500 nm height and 500 nm in diameter) has higher *EQE* than solar cell B1 (470 nm height and 700 nm in diameter), which most likely result from the higher surface area.

Nevertheless the solar cells with higher nanowires (B1 and B3) show much less *EQE* than the tiny nanostructures of sample B4 (see figure 4.15). It has to be mentioned that the planar solar cell shows better *EQE* than the solar cells with the higher nanowires.

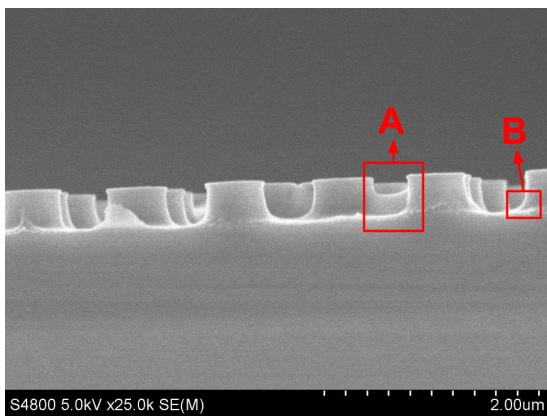


Figure 4.17: *SEM* image of the surface of sample B1

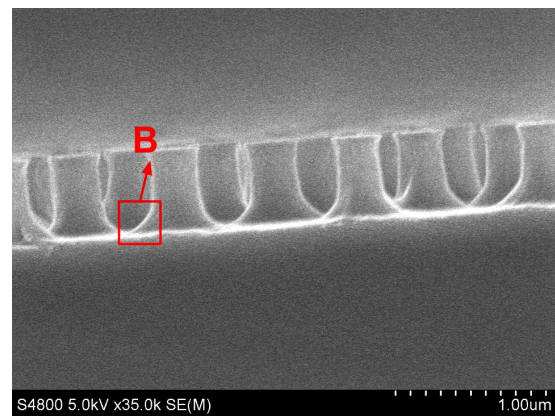


Figure 4.18: *SEM* image of the surface of sample B3

4.3. SPECTRAL RESPONSE OF THE DEVICE

This might be a result of bad wetting of the PEDOT:PSS layer on the silicon nanowires. In sample B4 the surface of the nanowires were completely coated with the polymer (see figure 4.19) whereas in sample B3 and B1 the polymer is not perfectly aligned on the surface (see figures 4.17 and 4.18). The region marked with "A" shows that the polymer only hangs between two nanowires. This might be because a too short distance between them. The region marked with "B" shows that it is hardly possible to coat the nanowires down to the bottom perfectly. On most wires the polymer bends away on the bottom.

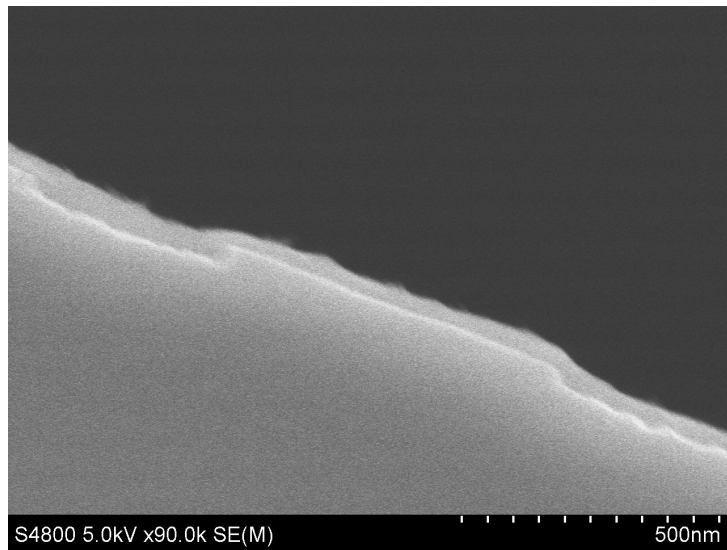


Figure 4.19: *SEM* image of the surface of sample B4

4.4 IV characteristics of the device

The I-V curve analysis is a powerful method for characterizing a solar cell. All IV measurements have been performed using AM 1.5G spectrum.

In figure 4.20 it can be seen that all nanostructured cells show higher J_{SC} than the planar solar cell. The higher J_{SC} results from the better reflective behavior of the nanostructured cell as well from the larger active area caused by the *SiNW*. As the solar cell with the smallest nanowires (B4) has the best antireflective behavior it shows the highest J_{SC} .

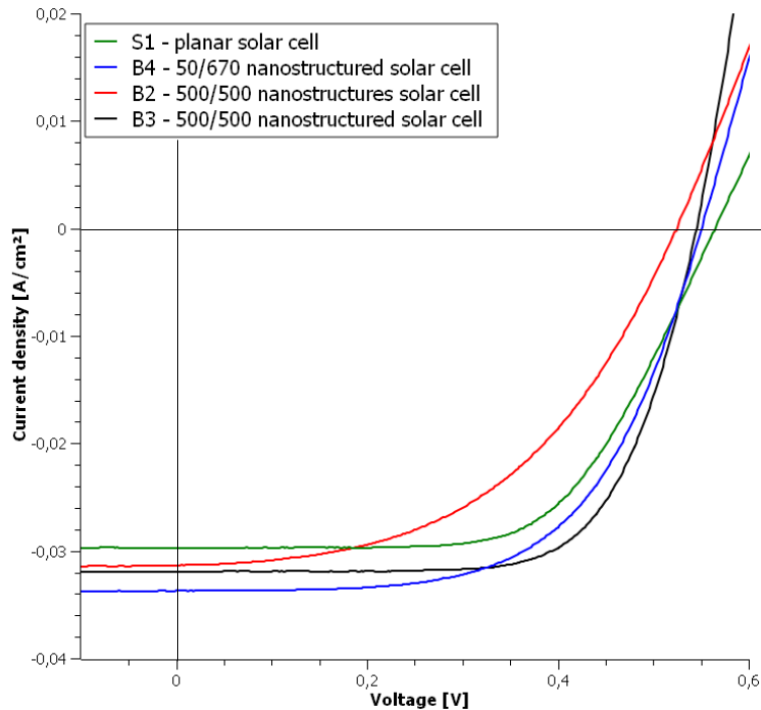


Figure 4.20: IV curve (AM 1.5G) of nanostructured solar cells compared to a planar solar cell (S1)

The V_{OC} is dependent on the saturation current (see equation 2.6) and therefore on the recombinations. As the recombinations of charge carriers increase the saturation current increase. The V_{OC} is inverse depended on the saturation current so it decreases with increasing saturation current.

The *SiNW* reduce the recombinations in the solar cell because there are radial organic-inorganic junctions. These junctions decrease the path the charge carriers have to travel to get to the electrodes and therefore minimize the probability of charge carrier recombi-

4.4. IV CHARACTERISTICS OF THE DEVICE

nations. So it is assumed that the nanostructured solar cells show higher V_{OC} than the planar solar cell. In table 4.1 it can be seen that the planar solar cell has the highest V_{OC} . This might be a result of voltage drops that produce leakage pathways in the nanostructured solar cells. In table 4.2 it can be seen that shunt resistance of the planar solar cell is worse than that of the solar cell with the best efficiency. It is not understood why the planar solar cells has the highest V_{OC} .

Table 4.1: Electric properties of the manufactured solar cells

Sample	$V_{OC}[mV]$	$J_{SC}[\frac{mA}{cm^2}]$	FF[%]	η [%]
S1 - planar solar cell	565	29.8	60.8	10.3
B4 - 50/670 nanostructured solar cell	551	33.7	59.7	8.0
B2 - 500/500 nanostructured solar cell	525	31.5	48.5	8.0
B3 - 500/500 nanostructured solar cell	545	31.9	68.5	11.9

The nanostructured solar cell B2 has the worst FF with only achieving 48.5%. This might be a result of parasitic resistances (see table 4.2). A low FF directly influences the efficiency. That is the major reason for the low efficiency of B2. The highest efficiency achieved was 11.9% for the B3 sample.

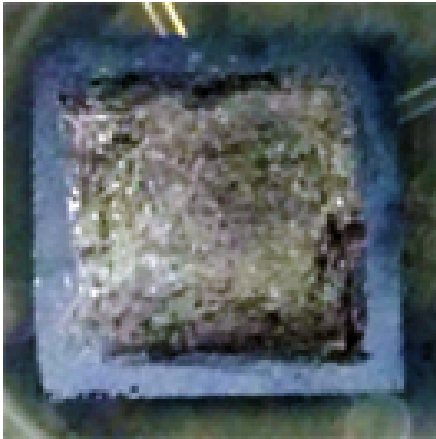


Figure 4.21: Photograph of the back contact of the planar solar cell S1

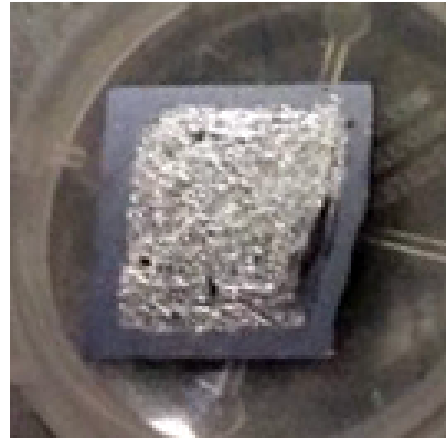


Figure 4.22: Photograph of the back contact of the 50/670 nanostructured solar cell B4

To get a better understanding of the IV-characteristics, the parasitic resistances have been calculated. As mentioned in section 2.3.2 the shunt resistance can be derived from the inverse curve at the I_{SC} point. Ideal solar cells show infinite R_{Sh} and the R_S being zero. The series resistance can be derived from the inverse curve at the V_{OC} point.

This table 4.2 shows that sample B2 has a much worse shunt resistance than sample B3. This means that the fabrication process of solar cell B2 has produced more defects

4.4. IV CHARACTERISTICS OF THE DEVICE



Figure 4.23: Photograph of the back contact of the 500/500 nanostructured solar cell B2



Figure 4.24: Photograph of the back contact of the 500/500 nanostructured solar cell B3

Table 4.2: Calculated parasitic resistance of solar cell

Sample	$R_{Sh}[\Omega cm^2]$	$R_S[\Omega cm^2]$
S1 - planar solar cell	16666.6	5.2
B4 - 50/670 nanostructured solar cell	2812	3.6
B2 - 500/500 nanostructured solar cell	416.6	5.1
B3 - 500/500 nanostructured solar cell	10000.0	2.3

and impurities and therefore a higher leakage current. The same explanation can be applied to the low R_{Sh} of B4 (50 nm high and 670 nm diameter nanowires). The series resistance of all samples are very low. The higher R_S of solar cells B2 and S1 probably result from the bad back contacts (see figure 4.23 and 4.21) compared to the better back contacts of solar cells B3 and B4 (see figure 4.22 and 4.24).

Chapter 5

Conclusion and outlook

In this work the nanostructures have been fabricated by a top down process. Hydroplaning was chosen as the process for coating the substrate with a mask of polystyrene microspheres. It is an easy and fast alternative to Langmuir-Blodgett troughs. After deposition the spheres can easily be shrunk with oxygen plasma to almost any size needed. Eventually, the nanostructures are produced using a *RIE* as this is a process that can easily be controlled and varied to get desired structures.

The nanostructured substrates are transformed into hybrid solar cells depositing a thin *PEDOT:PSS* layer around the *SiNW* using spin coating. This polymer does not only serve as the hole providing part of the solar cell but also functions as anti-reflective coating. Meaning that more light can be coupled into the solar cell and thus create electron hole pairs. The nanowire structuring with its *PEDOT:PSS* coating creates radial pn-junction which reduces the necessary diffusion length for the charge carries. So the probability of recombination losses can be reduced.

In general it can be said that nanostructures influence the solar cell behavior in a most positive way.

The nanostructured solar cell with the smallest nanowires (50 nm high and 670 nm in diameter) show the lowest reflectivity in the visible range (minimum of 17% reflectivity @466 nm). But the nanostructured cell with the highest nanowires (500 nm high and 500 nm in diameter) shows the best antireflective behavior in the near infrared range (minimum of 9% reflectivity @1041 nm). The samples with longer nanowires show a resonance behavior in the reflectivity spectra.

With 92% (@480 nm) external quantum efficiency the solar cell with the smallest nanowires shows the highest *EQE*. This solar cell shows not only a punctually higher

EQE than the other solar cells (including the planar solar cell) but its *EQE* is higher over the most part of the wavelength range. The nanostructured solar cells with longer nanowires show even worse *EQE* than the planar solar cell. This might be a result of the bad wetting of the PEDOT:PSS between the nanowires.

The nanostructured solar cells in general show higher short circuit current density than the planar solar cell. The solar cell with the tiny nanowires shows the highest J_{SC} with $33.7 \frac{mA}{cm^2}$. Nevertheless the planar solar cell shows the highest V_{OC} of all measurements with 565 mV. Due to the fill factor of under 60% for two of the nanostructured solar cells, including the solar cell with the tiny nanowires, their efficiencies are just 8%. For both solar cells the shunt resistance is very low, which might be the reason for the low fill factor. The planar solar cell achieves an efficiency of 10.3%. **The best efficiency being 11.9%** is achieved of a nanostructured solar cell with long nanowires (500 nm high and 500 nm diameter). This solar cell achieves the highest shunt resistance ($R_{Sh} = 100000.0 \Omega cm^2$) and the lowest series resistance ($R_S = 2.3 \Omega cm^2$) of all measured solar cells.

There are several investigation that might produce solar cells with even higher efficiencies. Following experiments are suggested:

- In order to get a better understanding of the influence of the *SiNW* length further samples should be fabricated with much longer nanowires.
- As the shape of the nanowires might have a great influence it would be great to produce different shapes and look at the difference. With the manufacturing process described above it would be easy to customize the nanowire shape.
- As the front contact shades much of the active area silver nanowires are suggest as a front contact. They function over the whole active area so the charge carriers do not have to travel far. As they are transparent they will not reflect the incoming light as much as the gold grid does.

List of Figures

1.1	Schematic showing the influence of <i>DMSO</i> on <i>PEDOT:PSS</i> ^[27]	1
1.2	Schematic of planar solar cell. The cell thickness L has to be larger than its optical thickness $\frac{1}{\alpha}$ ^[13]	2
1.3	Schematic of radial pn junction ^[13]	2
2.1	Efficiency chart of the best research cell efficiencies reported by NREL ^[4] .	4
2.2	Schematic energy diagram of the donor-acceptor interface ^[5]	5
2.3	Schematic operation scheme of a hybrid solar cell ^[24]	6
2.4	Schematic of the different stages of spin coating ^[2]	8
2.5	Schematic used for the calculation of the FF	10
2.6	Electrical circuit with shunt and series resistance ^[6]	11
2.7	Impact of the shunt resistance on the I-V curve ^[3]	12
2.8	Impact of the series resistance on the I-V curve ^[3]	12
2.9	Theoretical description of an <i>EQE</i> plot, including the main reason for losses ^[9]	13
3.1	Schematic hydroplaning process. a) the spheres are dribbled on the glass slide and onto the water. b) there they form a closepacked monolayer. c) the substrate is placed in the water and underneath the monolayer. d) then it is slowly and slightly tilted pulled out. e) the sample dries in a 45° angle to get rid of the remaining water and solvents	15
3.2	Basic working principle of a lithographing process ^[17]	18
3.3	Spectrophotometer	20
3.4	Solar simulator	20
3.5	<i>EQE</i> measurement system ^[12]	21
4.1	Too much water on the surface might form multilayer <i>lines</i> as seen in the <i>SEM</i>	22

4.2	<i>SEM</i> image of a monolayer of polystyrene spheres pointing out defects in the structure	23
4.3	Average diameter as a function of etching time measured in a <i>SEM</i>	23
4.4	image of the lentil-like shape of microspheres shrunk in oxygen plasma	24
4.5	<i>SEM</i> image of the <i>SiNW</i> after the nanospheres have been washed away	24
4.6	Linear behavior of the height of the <i>SiNW</i> considering the reactive ion etch time	24
4.7	<i>SEM</i> cross section image of a nanostructured sample coated with <i>PEDOT:PSS</i>	25
4.8	Photography of the front contact of a solar cell with nanostructures	26
4.9	Photography of the back contact of a finished solar cell	26
4.10	Reflectivity spectra of differently nanostructured <i>Si</i> wafer with and without <i>PEDOT:PSS</i> coating	27
4.11	Multiple reflections between air, <i>PEDOT:PSS</i> and <i>Si</i> reducing the total reflectivity	28
4.12	Absorption coefficient of <i>PEDOT:PSS:DMSO</i> ^[22]	29
4.13	Schematic resonance behavior of long <i>SiNW</i> and light coupled deep into the <i>Si</i>	30
4.14	Reflectivity spectra of differently nanostructured solar cells compared to a planar solar cell	31
4.15	<i>EQE</i> spectra of a planar solar cell compared to a nanostructured solar cell with tiny <i>SiNW</i>	32
4.16	<i>EQE</i> spectra of two nanostructured solar cells with high <i>SiNW</i>	33
4.17	<i>SEM</i> image of the surface of sample B1	33
4.18	<i>SEM</i> image of the surface of sample B3	33
4.19	<i>SEM</i> image of the surface of sample B4	34
4.20	IV curve (AM 1.5G) of nanostructured solar cells compared to a planar solar cell (S1)	35
4.21	Photograph of the back contact of the planar solar cell S1	36
4.22	Photograph of the back contact of the 50/670 nanostructured solar cell B4	36
4.23	Photograph of the back contact of the 500/500 nanostructured solar cell B2	37
4.24	Photograph of the back contact of the 500/500 nanostructured solar cell B3	37

List of Tables

3.1	<i>RIE</i> operating parameters used in the experiments	17
3.2	Composition of the polymer solution used in the experiments	19
3.3	Spin parameter used in the experiments	19
4.1	Electric properties of the manufactured solar cells	36
4.2	Calculated parasitic resistance of solar cell	37

Glossary

<i>CVD</i>	chemical vapor deposition
<i>DMSO</i>	dimethyl sulfoxide
<i>E-In/Ga</i>	indium gallium eutectic
<i>EQE</i>	external quantum efficiency
<i>FF</i>	fill factor
<i>HF</i>	hydrogen fluoride
<i>I_{SC}</i>	short circuit current
<i>J_{SC}</i>	short circuit current density
<i>PEDOT:PSS</i>	poly(3,4-ethylenedioxythiophene):poly(styrenesulfonate)
<i>RIE</i>	reactive ion etching
<i>SDS</i>	sodium dodecyl sulfate
<i>SEM</i>	scanning electron microscope
<i>SiNW</i>	silicon nano wires
<i>Si</i>	silicon
<i>V_{OC}</i>	open circuit voltage
<i>SF₆</i>	sulfur hexafluoride

Bibliography

- [1] Absorption depth. <http://pveducation.org/pvcdrom/absorption-depth>. Accessed: 2016-10-09.
- [2] Basic models of spin coating. <http://large.stanford.edu/courses/2007/ph210/hellstrom1/>. Accessed: 2016-06-14.
- [3] Dssc: Dye sensitized solar cells. <http://www.gamry.com/application-notes/physechem/dssc-dye-sensitized-solar-cells/>. Accessed: 2016-10-10.
- [4] Efficiency chart. <http://www.nrel.gov/ncpv/>. Accessed: 2016-10-10.
- [5] Energy diagram of charge separation at a donor-acceptor interface. https://en.wikipedia.org/wiki/File:Chargeseperation_mike.JPG. Accessed: 2016-10-02.
- [6] The equivalent circuit of a solar cell. https://en.wikipedia.org/wiki/Theory_of_solar_cells#/media/File:Solar_cell_equivalent_circuit.svg. Accessed: 2016-10-10.
- [7] German organic solar cell from heliatek is claiming a record conversion efficiency at 13.2% for multi-junction cell. <http://www.electronicweeky.com/market-sectors/power/record-organic-solar-cell-efficeincy-2016-02/>. Accessed: 2016-02-15.
- [8] Incident photon-to-current efficiency (ipce). <http://plasticphotovoltaics.org/lc/characterization/lc-advanced-c/lc-ipce.html>. Accessed: 2016-05-10.
- [9] Instrumentation for quantum efficiency measurement of solar cells. <http://www.renewableenergyworld.com/articles/2010/07/instrumentation-for-quantum-efficiency-measurement-of-solar-cells.html>. Accessed: 2016-08-02.

- [10] Organic solar cells. https://en.wikipedia.org/wiki/Organic_solar_cell. Accessed: 2016-10-10.
- [11] Panasonic hit solar cell achieves world's highest energy conversion efficiency of 25.6% at research level. http://eu-solar.panasonic.net/fileadmin/user_upload/News_PDFs/140410_Panasonic_HIT_E.pdf. Accessed: 2016-02-15.
- [12] Quantum efficiency measurement system. <https://www.newport.com/f/quantum-efficiency-and-ipce-measurement-kit>. Accessed: 2016-10-18.
- [13] Radial pn junction, wire array solar cells. http://thesis.library.caltech.edu/3702/1/Brendan_Kayes_Thesis.pdf. Accessed: 2016-07-28.
- [14] Refractive index of pedot:pss. https://www.iapp.de/iapp/agruppen/oled/index.php?Research_on_OLEDs:Alternative_Anodes. Accessed: 2016-05-18.
- [15] Refractive index of silicon. <http://www.filmetrics.de/refractive-index-database/Si/Silicon>. Accessed: 2016-05-18.
- [16] San jose solar company breaks efficiency record for pv. <https://www.kcet.org/redo/san-jose-solar-company-breaks-efficiency-record-for-pv>. Accessed: 2016-10-02.
- [17] Semiconductor fabrication: Photolithography. <http://britneyspears.ac/physics/fabrication/photolithography.htm>. Accessed: 2016-06-15.
- [18] Series resistance. <http://www.pveducation.org/pvcdrom/solar-cell-operation/series-resistance>. Accessed: 2016-10-10.
- [19] Solar simulator. https://en.wikipedia.org/wiki/Solar_simulator. Accessed: 2016-10-03.
- [20] C.A.J Ammerlaan, A. Chantre, and P. Wagner. *Science and Technology of Defects in Silicon*, page 265. North-Holland, 1989.
- [21] J. C. BERNEDE. Organic photovoltaic cells: History, principle and techniques. *Journal of the Chilean Chemical Society*, (3):1549–1564, 2008.

- [22] J Gasiorowski, R Menon, K Hingerl, M Dachev, and Sariciftci NS. Surface morphology, optical properties and conductivity changes of poly(3,4-ethylenedioxythiophene):poly(styrenesulfonate) by using additives. *Thin Solid Films*, 2013.
- [23] M. A. Green, K. Emery, Y. Hishikawa, W. Warta, and E. D. Dunlop. Solar cell efficiency tables (version 46). *Progress in Photovoltaic*, 2015.
- [24] Matthias Mattiza, Sara Jaeckle, and Silke Christiansen. Interface investigation of planar hybrid n-si/pedot:pss solar cells with open circuit voltages up to 645 mv and efficiencies of 12.6%. *Applied Physics*, (4), 2014.
- [25] Tsai Meng-Lin, Wei Wan-Rou, Tang Libin, Chang Hung-Chih, Tai Shih-Hsiang, Yang Po-Kang, Lau Shu Ping, Chen Lih-Juann, and He Jr-Hau. Si hybrid solar cells with 13% efficiency via concurrent improvement in optical and electrical properties by employing graphene quantum dots. *ACS Nano*, 2016.
- [26] Kwang-Tae Park, Han-Jung Kim, Min-Joon Park, Jun-Ho Jeong, Jihye Lee, Dae-Geun Choi, Jung-Ho Lee, and Jun-Hyuk Choi. 13.2% efficiency si nanowire/pedot:pss hybrid solar cell using a transfer-imprinted au mesh electrode. *Scientific Reports*, 2015.
- [27] Matthias Pietsch, Muhammad Y. Bashouti, and Silke Christiansen. The role of hole transport in hybrid inorganic/organic silicon/ poly(3,4-ethylenedioxythiophene):poly(styrenesulfonate) heterojunction solar cells. *The journal of physical chemistry*, pages 9049–9055, 4 2013.
- [28] M. Singh, TR. Rana, S Kim, K. Kim, JH. Yun, and Kim. J. Silver nanowires binding with sputtered zno to fabricate highly conductive and thermally stable transparent electrode for solar cell applications. *ACS Applied Materials Interfaces*, 8, 2016.
- [29] Loucas Tsakalacos, Joleyn Balch, Jody Fronheiser, Min-Yi Shih, Steven LeBoeuf, Mathew Pietrzykowski, Peter Codella, Bas Korevaar, Oleg Sulima, Jim Rand, Anilkumar Davuluru, and Umakant Rapolc. Strong broadband optical absorption in silicon nanowire films. *Journal of Nanophotonics*, 1, 7 2007.
- [30] Nicolas Vogel, Sebastian Goerres, Katharina Landfester, and Clemens K. Weiss. A convenient method to produce close- and non-close-packed monolayers using direct

assembly at the air–water interface and subsequent plasma-induced size reduction. *Macromolecular Chemistry and Physics*, 212:1719–1734, 8 2012.

- [31] Danbei Wang, Weixin Zhou, Huan Liu, Yanwen Ma, and Hongmei Zhang. Performance improvement in flexible polymer solar cells based on modified silver nanowire electrode. *Nanotechnology*, 27(33), 2016.
- [32] Ge Zhaoyun, Xu Ling, Cao Yunqing, Wu Tao, Song Hucheng, Ma Zhongyuan, Xu Jun, and Chen Kunji. Substantial improvement of short wavelength response in n-sinw/pedot:pss solar cell. *Nanoscale Research Letters*, 2015.